Carrageenan based printable magnetic nanocomposites for actuator applications

V. M. Macedo[1], N. Pereira[2,3], C. R. Tubio[1], P. Martins[2,4], C. M. Costa[2,4,5,*] and S. Lanceros-Mendez[1,6,*]

[1]BCMaterials, Basque Center for Materials, Applications and Nanostructures, UPV/EHU Science Park, 48940 Leioa, Spain

[2]Physics Centre of Minho and Porto Universities (CF-UM-UP), University of Minho 4710-053 Braga, Portugal

[3]Centro ALGORITMI, University of Minho, Campus de Azurém, 4800-058 Guimarães, Portugal

[4]Laboratory of Physics for Materials and Emergent Technologies, LapMET

[5]Institute of Science and Innovation for Bio-Sustainability (IB-S), University of Minho, 4710-053 Braga, Portugal

[6]Ikerbasque, Basque Foundation for Science, 48009 Bilbao, Spain

***Corresponding Authors** Email: C. M. Costa (cmscosta@fisica.uminho.pt); S. Lanceros-Méndez (senentxu.lanceros@bcmaterials.net)

Abstract:

The digitalization of the society in the context of the Internet of Things (IoT) demands a new generation of sustainable materials and processes to reduce the environmental impact of technological advances. This work reports on sustainable multifunctional nanocomposites based on carrageenan and magnetic cobalt ferrite ($CoFe_2O_4$-CFO) nanoparticles, processed by direct-ink-writing and on their applicability as magnetic actuators. The nanocomposites exhibit a compact morphology with CFO nanoparticles well distributed within the polymer matrix. The incorporation of CFO nanoparticles

significantly improves the thermal and mechanical properties of the polymer: the onset degradation temperature increases 30ºC and the Young's modulus increases from 1 MPa in the pristine polymer to 17 MPa for the composite with 5 wt.% CFO content. CFO magnetic nanoparticles are also responsible for increasing the dielectric constant of carrageenan from ≈1000 up to ≈9000 (10wt.% CFO composite), and for the magnetic properties, with a maximum magnetization of ≈16 emu.g^{-1} and coercive field of ≈3.4 kOe in the 30 wt.% CFO composite. A magnetic actuator has been developed with excellent maximum displacement.

Keywords: A. Nano composites; A. Polymer matrix composites (PMCs); A. Smart materials; B. Magnetic properties; E. 3D printing

1. Introduction

The Internet of Things (IoT) has the broad vision of interconnecting every single object within an interactive network [1]. Electronic devices, including radio-frequency identification (RFIDs), memory devices, power sources, sensors and actuators, together with the communication and computation technologies, are basis of the IoT. Currently, the technological development of electronic materials continues focusing on miniaturization and improved device integration, with lower energy consumption and smart capabilities [2]. Further, the increasing demand and use of electronic materials based on rapid economic and social changing scenarios, results in tons of electrical and electronic waste (e-waste) every year [3]. This waste represents a global challenge to manage, that has not been properly addressed, the e-waste contamination representing a huge impact for ecological environment and public health [3]. Printed electronics has the potential to minimize the amount of excessive chemicals involved in the manufacturing of specific electronics systems as well as lower energy consumption, allowing also the

development of electronic solutions based on environmentally friendly materials [4]. One of the main trends in this scenario is the development of biodegradable electronics based on natural and/or biodegradable materials. A variety of biodegradable materials have been used as substrates for printed electronics including leather, silk, hot-pressed cotton-fibre paper and, in particular, cellulose [6], so a next step needs to include the development of sustainable printable inks with tailored properties for advanced electronics [7]. This is interesting not only from an environmental point of view, but also from an economic perspective, since biodegradable materials typically present lower production costs [8].

Thus, biopolymer and biodegradable polymer have been used to this end based on environmental friendly printable inks [9]: cellulose for conductive [10] and magnetic [11] inks, PLLA for conductive inks [12], chitosan with magnetic nanoparticles for resistive sensor [13] or among others.

Among the different possible biodegradable materials, carrageenan has interesting features, including low-cost, abundance, water-solubility, non-toxicity and biodegradability [14-16]. Carrageenan is a natural sulphated and anionic polysaccharide (carbohydrate), extracted from the multicellular wall of certain species of red algae seaweeds of the *Rhodophyceae* family [14, 17], such as Chondrus crispus, Gigartina, Euchuema and Hypnea. Another interesting properties of this polymer include gelling, thickening, emulsifying, stabilizing, anticancer, anticoagulant, antihyperlipidemic and immunomodulatory properties [18]. Furthermore, three main types of carrageenan can be found: kappa (κ), iota (ι), and lambda (λ), with sulfate contents of 20 w/w%, 33 w/w% and 41 w/w%, respectively [16, 19]. Carrageenan has been traditionally used in the food industry as fat substitute in milk products as well as in the textile, printing, pharmaceutical and cosmetic industries [20]. The gels formed by iota-carrageenan are elastic with good freeze, thaw and healing properties [21]. Iota-carrageenan adds chemical stability and

antiviral activity to carrageenan-based devices, making this polysaccharide very promising for IoT-related applications [22, 23]. Carrageenan has a physical aspect of powder at pure and dry form, with no smell and no taste; it is translucid and when added into solutions there is no change in the original colour. Further, it has the capability to create water-retaining hydrogels that can be processed by 3D printing [24].

Thus, in the scope of technological applications, carrageenan has been used for the development of electrochemical devices [15], primary proton batteries [25], dye-sensitized solar cells [26] and optical sensors [27].

From all required technologically enabling materials, magnetoactive materials are particularly interesting since they allow the fabrication of sensors and actuators that can be wirelessly triggered, very useful for the digitalization of society in topics such as antennas, magnetic-sensing/actuation and motion-sensing/actuation applications, among others [28]. Magnetoactive materials are often produced in the form of nanocomposites by combining magnetic fillers within a polymeric matrix [29], leading also to magnetoelectric effects when the magnetic materials are combined with electroactive polymers [5]. Cobalt ferrite ($CoFe_2O_4$-CFO) nanoparticles have been extensively used for the development of magnetoactive polymer composites due to their low cost, high chemical stability, high mechanical hardness and strength, high coercivity, wear anisotropy, high saturation magnetization, high-temperature magnetic order (520 °C), large magneto crystalline anisotropy constant and high Curie temperature [30-33]. In addition to carbon nanotubes (CNTs), their magnetic properties are enhanced [34] and they can also be used as a Cr-VI sensor in water [35].

Furthermore, compared to other magnetic nanoparticles, such as $NiFe_2O_4$ or $ZnFe_2O_4$, CFO nanoparticles show large magnetization and magnetostriction, low eddy-current

losses and considerable electrical resistance with low dielectric loss [31]. Further, CFO can be produced by Green Synthesis, in the scope sustainable approaches [36].

Thus, this work reports on the development of magnetoactive nanocomposites by additive manufacturing based on Iota-Carrageenan with embedded cobalt ferrite (CFO) nanoparticles using water as solvent and processed by 3D printing technique, being therefore an step forward towards reducing environmental impact when compared with magnetic sensor based on poly(vinylidene fluoride-trifluoroethylene)/cobalt ferrite (P(VDF-TrFE)/CFO) [37] or poly(3,4-ethylenedioxythiophene), PEDOT/CFO [38], while maintaining high performance. The morphological, thermal, mechanical, electrical and magnetic properties of the developed materials are addressed together with their implementation into a magnetic actuator.

2. Experimental details

2.1.Materials

Iota-Carrageenan was purchased from *Alfa Aesar* into powder form. Ultrapure water was obtained from a Milipore-Q system. $CoFe_2O_4$ (CFO) nanoparticles with 35–55 nm particle size, were purchased from NanoAmor. The surfactant Triton X-100 (aqueous) was purchased from Sigma-Aldrich.

2.2.Nanocomposite ink preparation

The manufacturing process of the nanocomposites is represented in Figure 1. The solution of pure Iota-Carrageenan was produced by dissolution of 3 wt.% of the polymer in ultrapure water at ambient temperature, under magnetic stirring. The mixtures of Iota-carrageenan and $CoFe_2O_4$ (CFO) nanoparticles (NPs) were produced with concentrations of 0.5 wt.%, 1 wt.%, 5 wt.%,10 wt.%, 20 wt.% and 30 wt.% CFO NP content with respect to the carrageenan content. To prepare the composites, first, the surfactant (0.01wt.%) was added into the ultrapure water (Step 1) to assist NPs dispersion. Then, the

nanoparticles were added, and the dispersion was placed in an ultrasonic bath for 3 hours (Step 2) to achieve nanoparticle surfactation. Finally, Iota-Carrageenan solution was added and mixed under mechanical stirring for another 3 hours (Step 3).

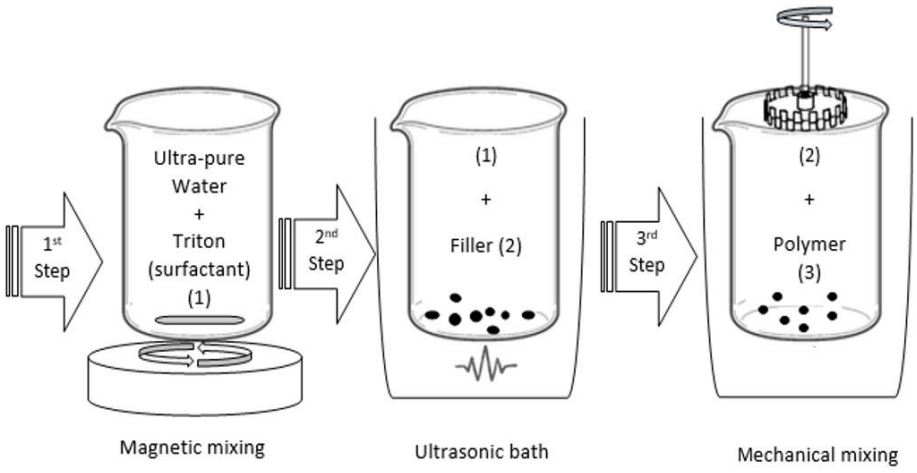

Figure 1 – Schematic representation of the preparation of the nanocomposite ink.

2.2.1. Direct-ink printing

The developed ink was transferred to a syringe and isolated with parafilm on the entrance of the piston and on the entrance of needle with a polymeric stopper. Then, the syringe was centrifuged at 2500 rpm for 15 minutes in order to remove the bubbles within the ink. Next, the piston was inserted back into the syringe and placed into the bioprinter Single Head 3D Bioprinter (3D Cultures). The printing parameters were: needle diameter of 0.41 mm, space line of 0.51 mm (to avoid overlay of lines on the same plane), printing speed of 30 $mm.s^{-1}$ and extrusion multiplier of 0.008.

2.3. Samples characterization

The morphology of the CFO/Carrageenan nanocomposites was evaluated by Scanning Electron Microscopy (SEM), NanoSEM – FEI Nova 200 (FEG/SEM)). Before analysis, the samples were coated by magnetron sputtering with a conductive gold layer (Polaron SC502 apparatus).

The dispersion and distribution of CFO nanoparticles within the carrageenan matrix was analyzed by Energy Dispersive X-Ray Analysis (EDX) (Hitachi Tabletop Microscope TM 3000).

Fourier transformed infrared spectroscopy (FTIR) was performed at room temperature in the attenuated total reflection (ATR) mode with a Jasco FT/IR-4100 system. Measurements were performed between 600 cm^{-1} and 4000 cm^{-1} using 64 scans with a resolution of 4 cm^{-1}.

Thermal properties of the CFO/Carrageenan nanocomposites were accessed by Differential Scanning Calorimetry (DSC) and Thermogravimetric Analysis (TGA). DSC scans were carried out using a Mettler Toledo DSC 822e equipment with a sample robot, under nitrogen flow of 50 ml/min between 20 ºC and 150 ºC at 10 ºC/min. The samples weight used in the test was between 6 and 10 mg.

TGA thermograms were obtained with a TGA/SDTA 851e Metter Toledo Apparatus from 30 °C to 600 °C at a rate of 10 °C/minute with a nitrogen flow rate of 50 $ml.min^{-1}$.

The mechanical properties of the CFO/Carrageenan nanocomposites were evaluated at room temperature under tensile stress with a Linkam Scientific Instruments TST 360 at a constant deformation of 50 $\mu m.s^{-1}$.

Dielectric measurements were performed at room temperature with a Quadtech 1920 LCR precision meter. The capacity (C) and tan δ were obtained in the frequency range from 20 Hz to 1 MHz with an applied voltage of 0.5 V. In each film, circular gold electrodes with 5 mm diameter were deposited onto both sides in the form of a parallel

plate condenser. The real and imaginary part of the dielectric function (ε' and ε''), respectively and real part of the conductivity (σ') were determined through the following equations:

$$\varepsilon' = \frac{C.d}{\varepsilon_0.A} \quad (1)$$

,

$$\varepsilon'' = tan\,\delta * \varepsilon' \quad (2)$$

and

$$\sigma'(\omega) = \varepsilon_0 \omega \varepsilon''(\omega) \quad (3)$$

where *C* is the capacitance (F), ε_0 is the permittivity of free space, A is the electrode area (m^2), d is the thickness of the samples and $\omega = 2\pi f$ is the angular frequency [39].

The magnetic properties of the CFO/Carrageenan composites were measured with a Micro-Sense EZ7 Vibrating Sample Magnetometer (VSM) from -18 kOe to 18 kOe. The temperature dependent magnetic response of the CFO/Carrageenan nanocomposite with 30 wt.% was studied at 20, 50, and 100 ºC.

2.4.Magnetic actuator development

The magnetic actuator device was produced with the CFO/Carrageenan nanocomposite with 30 wt.% CFO content.

Hi-Strength 90 spray adhesive from 3M was used for contact bounding between a 52 μm thick commercial poly(vinylidene fluoride) PVDF metalized film from measurement Specialties, Inc, due to high electro-mechanical conversion effect, and the magnetic CFO/carrageenan nanocomposite film. The electronic acquisition system was connected

to the electrodes of the PVDF film. Figure 2 shows the schematic representation of the data acquisition system (Figure 2a) together with images of the actuation set-up (Figure 2b). In Figure 2a, the black film represents the CFO/carrageenan nanocomposite and the blue film represents the PVDF film with the corresponding conductive electrodes in white.

Figure 2b) shows the test setup for the magnetic actuator. A NdFeB magnet (N45, 10 mm diameter, 5 mm thickness, KJ Magnetics) was used for creating the external magnetic field. The magnet was attached to a solenoid in order to vary the magnetic field frequency in the frequency range from 0.8 Hz to 2.5 Hz, by controlling the state of the solenoid (On /Off). The bending tests were performed by moving a NdFeB magnet close to the sample and registering the bending distance of the tip to the initial position of the sample and the magnetic field (Hall probe, Hirst magnetic instruments, gm08 Gaussmeter).

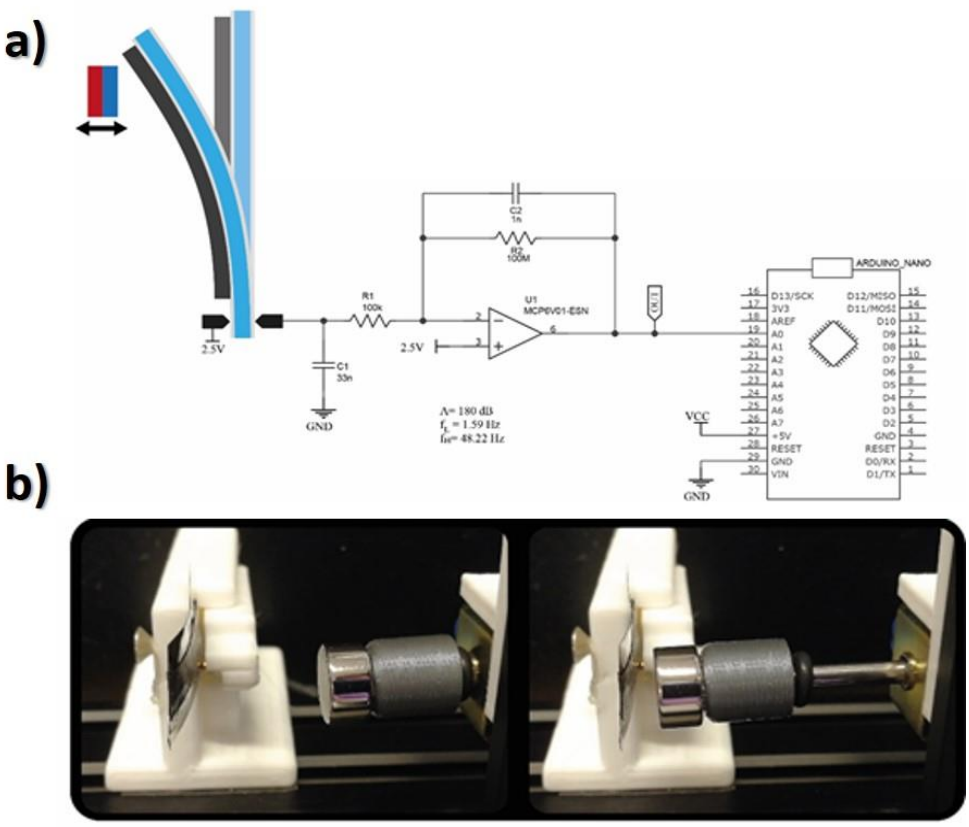

Figure 2 – a) Schematic representation of the sample and the electronic acquisition system. With respect to the sample, the black film represents the CFO/carrageenan nanocomposite and the blue film represents the PVDF film with the corresponding conductive electrodes in white b) magnetic actuation through a varying magnetic field applied by a moving magnet.

The electronic acquisition circuit is composed by a charge amplifier connected to the analog-to-digital converter (ADC) of an Arduino nano (ATMEGA328P). The data is sent via Universal Serial Bus (USB) where an application developed in Qt 5 plots the actuator response as shown in Figure 2a), when a magnet is approached to the sample. The charge amplifier integrates the input current and provides a voltage output proportional to the force applied to the piezoelectric material [40] via the bending induced by the applied magnetic field. This circuit reduces the input noise when compared to voltage sensing. The low-pass filter composed by the resistance R_1 (100 kΩ) and capacitor C_1 (33 nF) provides immunity to high frequencies and anti-aliasing filtering. The high pass filter, composed by the resistance R_2 (100 MΩ) and the capacitor C_2 (1 nF), limits the minimum input frequency. The reference voltage of 2.5 V provides a positive voltage offset that centers the output voltage at 2.5 V allowing the signal to be read by the microprocessor ADC.

3. Results and discussion

3.1.Morphological analysis

The morphology of the CFO/Carrageenan nanocomposites prepared by direct ink writing is presented in Figure 3. Regardless of the CFO content, a compact morphology of the carrageenan film is observed, as demonstrated by the representative cross-section images presented in Figure 3d.

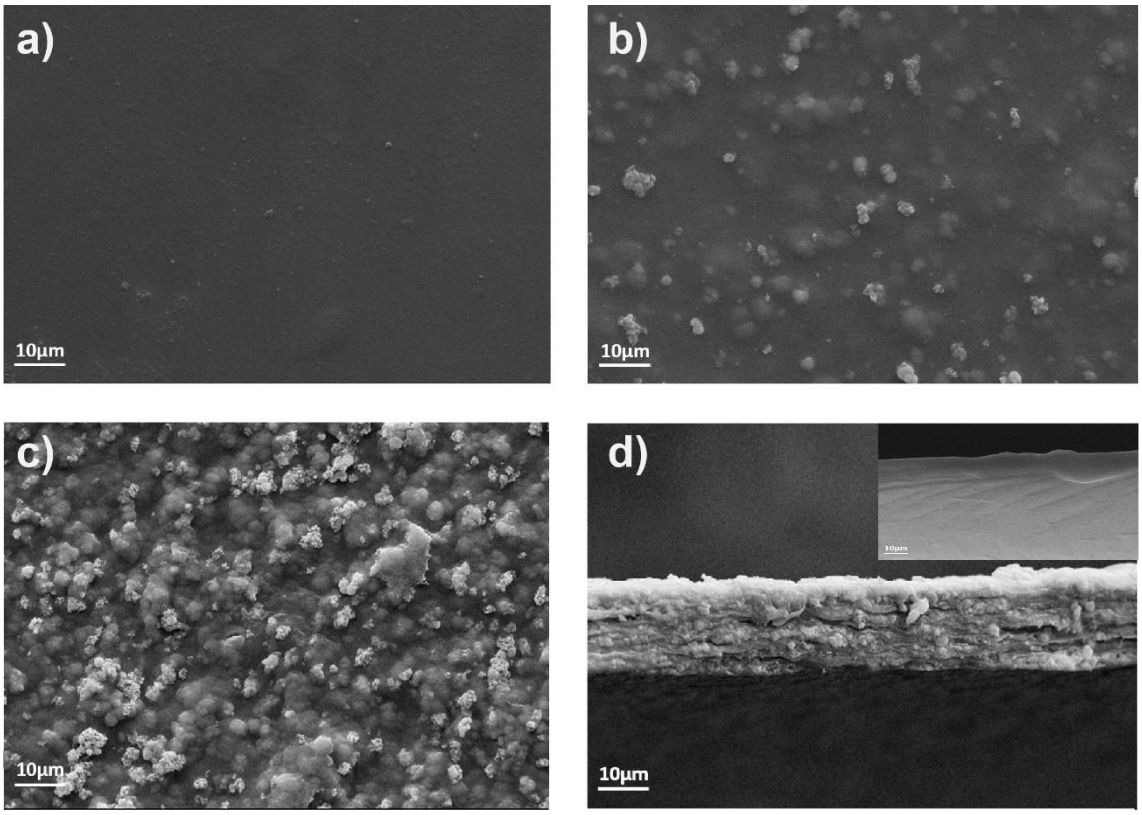

Figure 3 – SEM surface images of a) neat carrageenan, b) carrageenan composite with 0.5 wt.% CFO content, c) carrageenan with 30 wt.% CFO. SEM cross-section images for d) carrageenan with 30 wt.% CFO filler content (insert of neat carrageenan).

It is observed that for low filler contents (Figure 3b), the CFO nanoparticles are dispersed throughout the polymer matrix without detectable agglomeration. This observation is supported by the image of 0.5 wt.% CFO (figure 3b). For higher CFO content (30 wt.%), surface and cross-section images Figures 3c and 3), show well distributed agglomerates of CFO nanoparticles. Considering the different chemical elements that compose the CFO nanoparticles, Figure 4a-d shows the EDX mapping images for Fe and Co elements from different CFO/Carrageenan composites (5 wt.% and 30 wt.% CFO). Regardless of the CFO content in the polymer matrix, these elements are detected in all composites and confirm the good distribution of the particles within the polymer matrix, though some well dispersed agglomerates are detected for the samples with higher filler contents, as

shown in the 30 wt.% of CFO content sample (figure 4b). The same observations are found for the Co element (Figure 4c-d).

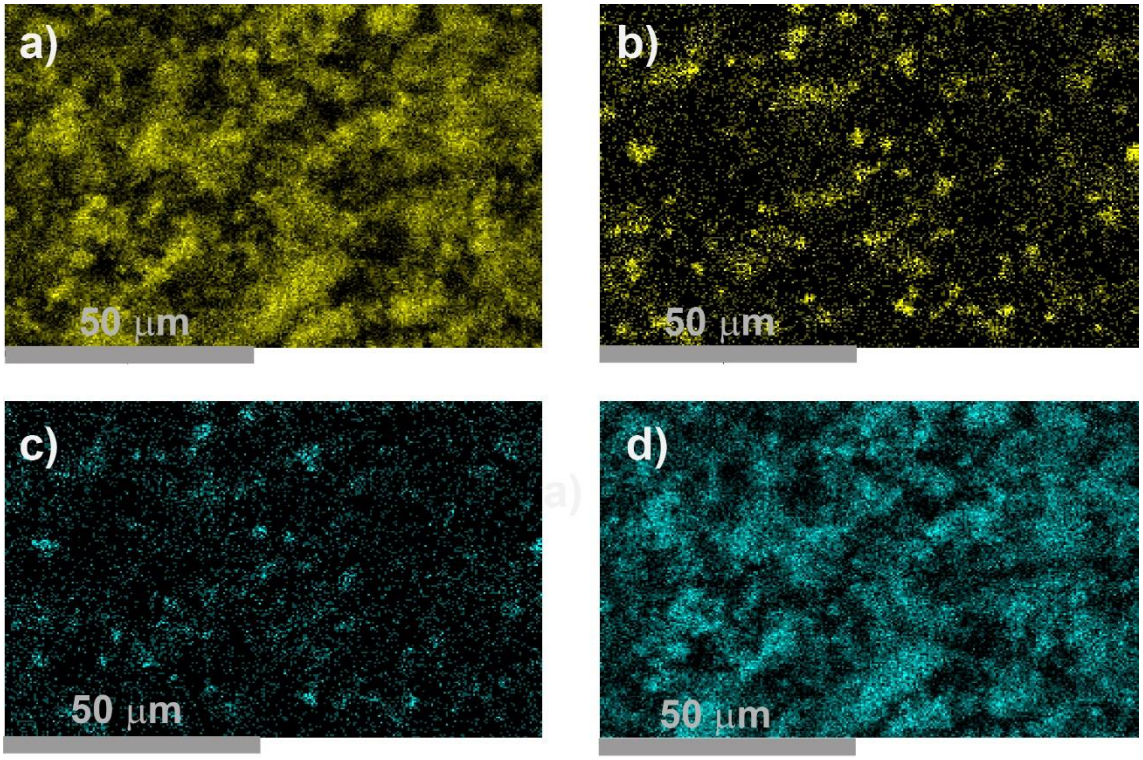

Figure 4 - EDX mapping images for Fe (iron, yellow) for samples with a) 5 wt.% of CFO and b) 30 wt.% of CFO and for Co (cobalt, blue) for samples with: c) 0.5 wt.% of CFO and d) 30 wt.% of CFO filler addition.

From SEM and EDX images (Figure 3 and 4), it is thus proven that it is possible to produce CFO/Carrageenan composites by direct-ink writing with compact microstructure and good dispersion/distribution of CFO nanoparticles.

3.2.Physical-chemical, thermal and mechanical properties

In order to evaluate the possible interactions between the CFO nanoparticles and the carrageenan polymer, Figure 5a shows the FTIR-ATR spectra for neat carrageenan and CFO/carrageenan nanocomposites with different CFO contents.

In all samples can be observed the typical vibration bands of carrageenan at 805, 1070, 1635 and 3400 cm^{-1} which correspond to the C-O-SO_3 bonds of 3,6-anyhydrogalactose in

C2 of the galactose unity, C-O bond of 3, 6-anyhydrogalactose, the C=O asymmetric stretch/N-H deformation and the OH/NH stretching band, respectively [41, 42].

Regarding the vibration bands of the CFO nanoparticles, only one is slightly detected: the one around 603 cm^{-1}, which corresponds to the Fe-O bond [43].

Figure 5b shows the DSC scan for neat carrageenan and the CFO/Carrageenan composites. An endothermic peak is observed around 100-120 °C, that is related to the superposition of the two effects: glass transition (Tg) of carrageenan [15, 25] and intrinsic water removal. A peak shift to high temperatures (106 ºC-120ºC) is observed for the nanocomposites with respect to neat carrageenan (100 ºC).

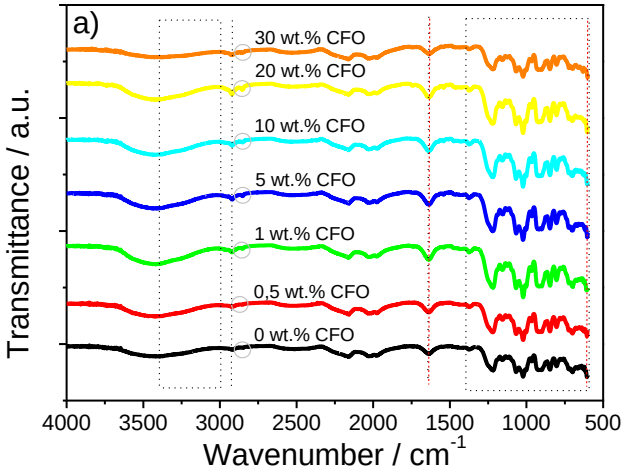

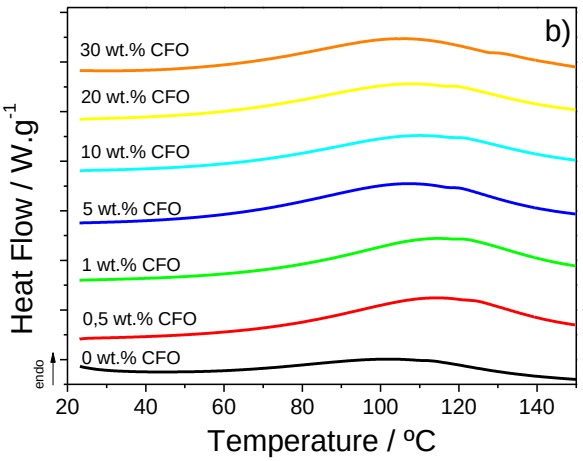

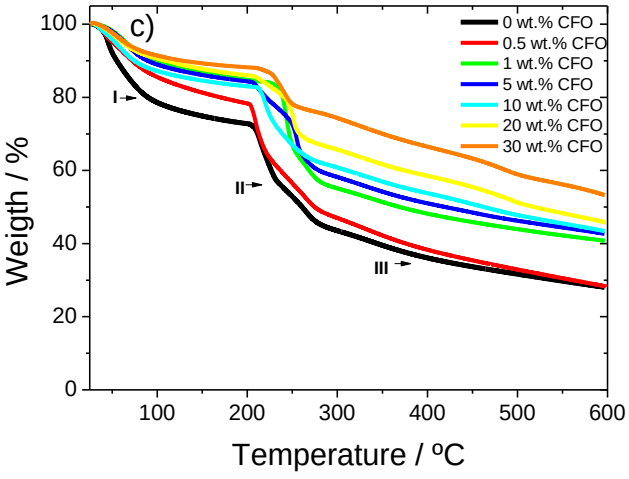

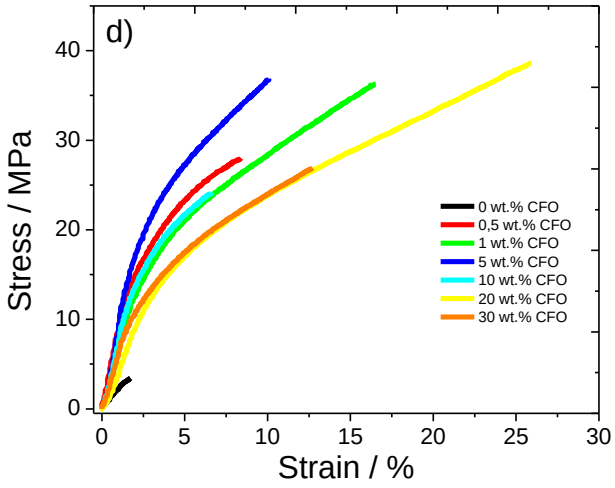

Figure 5 - a) FTIR-ATR spectra, b) DSC scans, c) TGA thermograms and d) Stress-Strain curves for neat carrageenan and the corresponding CFO/Carrageenan nanocomposites.

Figure 5c) shows the TGA thermogram for neat carrageenan and CFO/Carrageenan composites with different CFO contents. Neat carrageenan shows a first mass loss of ≈27% associated to moisture evaporation, that occurs from 14 °C to 114 °C . It is to notice that the initial mass loss decreases with increasing filler content, which may be related to water trapping nearby the fillers and/or within the particle agglomerates due to the dipolar interaction between water molecules and the nanoparticles surface [44]. Thus, the weight loss form that water can be detected at higher temperatures. The second weight loss (≈28%) occurs from 206 °C to 282 °C and is realted to carrageenan degradation [45]. Around these temperatures the decomposition of Triton X-100 should also happen, but due to its lower wt.% (< 10%) in the nanocomposites it does not have a significant impact on the thermogram [46].

Regarding the mechanical properties, figure 5d shows the stress-strain curves for neat carrageenan and the corresponding CFO/Carrageenan nanocomposites.

The typical mechanical curve of the carrageenan polymer [47] is observed in Figure 5d, the addition of CFO content improving the mechanical response (tensile strength and break) of the nanocomposites, the CFO nanoparticles acting as a mechanical reinforcement [48].

The Young's Modulus for the different CFO/carrageenan composites was evaluated from the linear regime at 2% of maximum elongation in the elastic region using the tangent method. It is observed that the Young Modulus does not increase linearly as a function of the CFO content, the CFO/carrageenan nanocomposite with the highest Young's modulus and yield strength being the sample with 5 wt.% of CFO (17 and 26 MPa, respectively),

compared to neat carrageenan (1 MPa and 4 MPa, respectively). For higher CFO contents (10, 20 and 30 wt.%), the mechanical properties of the composites (Young modulus and Yield strength) start to decrease, due to the agglomeration of the nanoparticles that act as defective structures and stress accumulation regions.

3.3.Dielectric properties

The real part of the dielectric constant (ε′) and a.c. electrical conductivity (σ′) are shown in figure 6 and allow to determine the effect of CFO content on the carrageenan polymer matrix and water boundary trapping. It is observed that the addition of CFO nanoparticles in the carrageenan polymer increases the dielectric properties of the matrix.

For neat carrageenan, and independently of the CFO content in the composites, ε′ (figure 6a) decreases with increasing frequency due to the limited dipolar mobility and corresponding dipole relaxation process [49].

Furthermore, independently of the frequency, ε′ increases with increasing CFO content once the presence of the fillers increases the interfacial and space charge polarization at the boundary of the fillers and the sample-electrodes interface (Maxwell−Wagner-Sillars effect) [50].

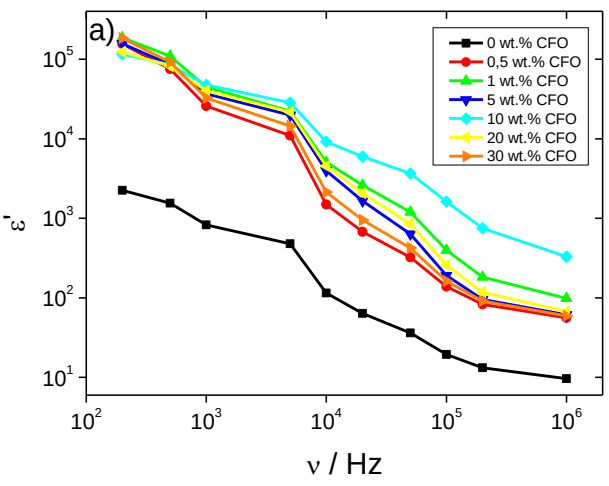

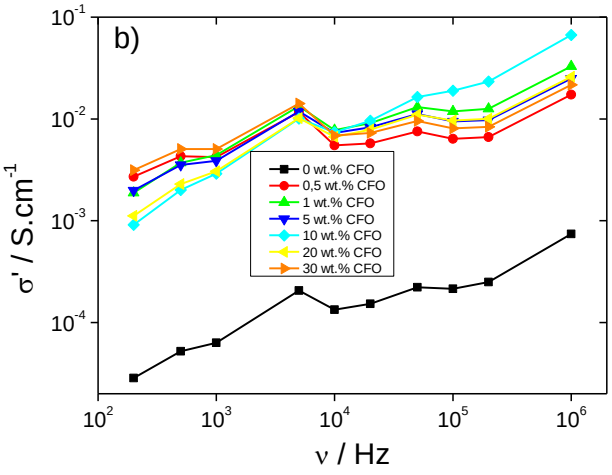

Figure 6 - (a) ε′ and (b) σ′ as a function of frequency for neat carrageenan and CFO/carrageenan nanocomposites.

Furthermore, regardless of frequency, it is observed that the addition of CFO nanoparticles in the carrageenan polymer matrix increases the a.c. electrical conductivity σ′ (Figure 6b), which increases with increasing frequency, indicating the contribution of the interfacial effects to the improvement of the electrical conductivity [51].

3.4.Magnetic properties

The magnetic properties of the CFO/Carrageenan nanocomposites were evaluated after the magnetic hysteresis loops (Figure 7a) showing the typical ferromagnetic hysteresis loops of CFO.

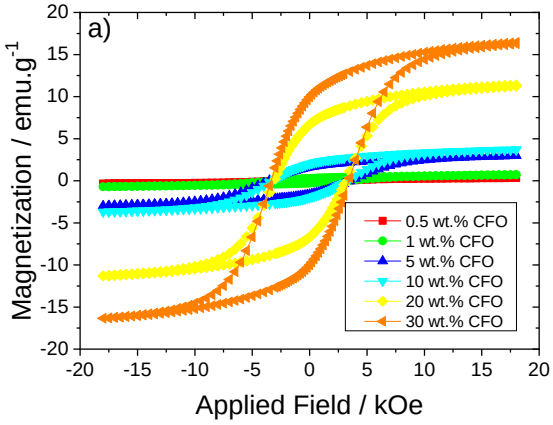

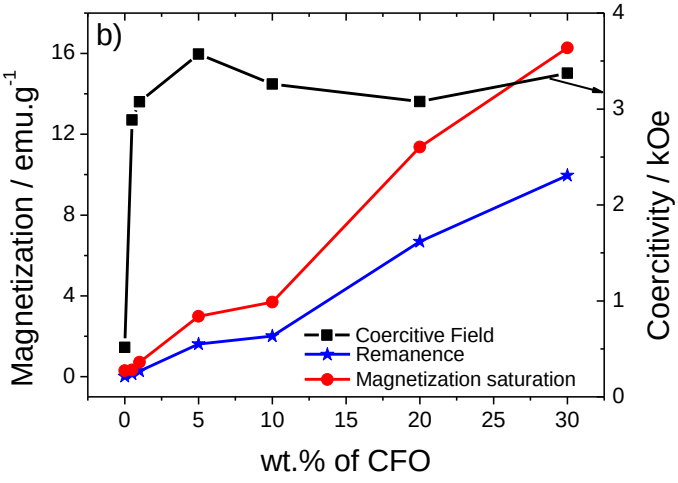

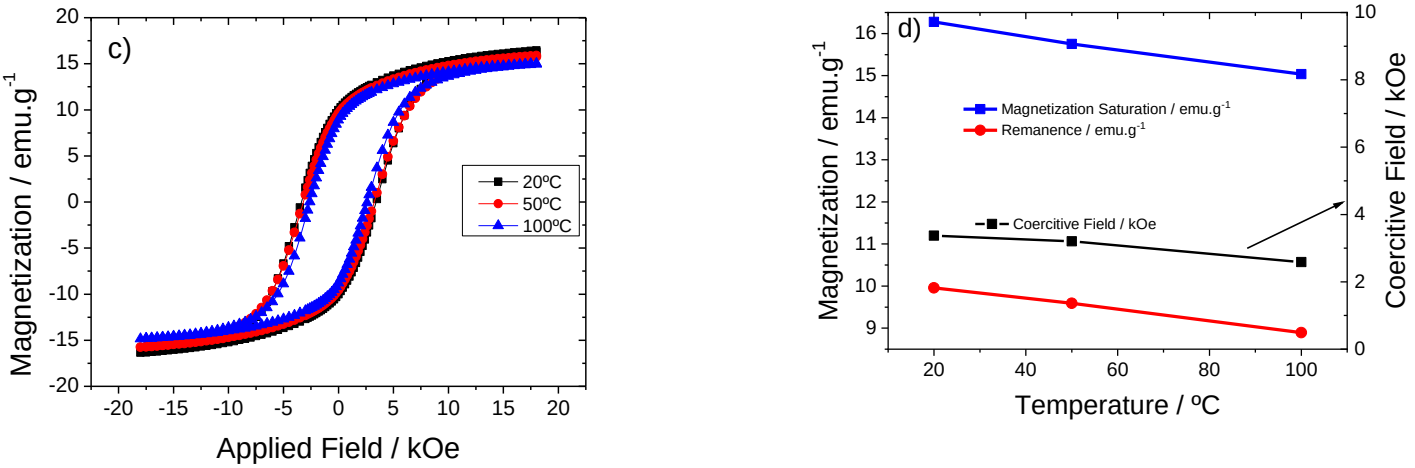

Figure 7 - a) Magnetic hysteresis loops for CFO/carrageenan nanocomposites at room temperature, b) saturation magnetization, remnant magnetization and coercive field obtained from the corresponding hysteresis loops. c) Hysteresis loops for the 30 wt.% CFO sample at different temperatures and d) corresponding temperature dependence of the saturation magnetization, remnant magnetization and coercive field.

It is observed that the magnetic behavior (saturation magnetization and remanence) of CFO/carrageenan nanocomposites depends on the CFO content, the hysteresis loops preserving the original ferromagnetic shape, independently of filler content [52]. Figure 7b shows the saturation magnetization M_s, magnetic field remanence and coercive field obtained from the magnetic hysteresis loops of figure 7a). The saturation magnetization and remanence increase with the addition of CFO nanoparticles in the carrageenan polymer matrix due to the increase of magnetic entities in the nanocomposite [53]. Also, the coercive field of the nanocomposites increases with CFO fillers addition up to 3.6 kOe at 5 wt.% CFO, remaining practically constant for increasing CFO content.

From the magnetic hysteresis loops of Figure 7a, the effective concentration of nanoparticles within the polymer matrix is calculated (Table 1), taking into consideration the saturation magnetization of CFO NPs (60 emu·g^{-1}) [54] and equation 4 [55]:

$$\%CFO = \frac{saturation\ magnetization\ (film)}{saturation\ magnetization\ of\ CFO\ NPs} \times 100, \quad (4)$$

Table 1 – Calculated effective CFO filler content within the samples, calculated after Equation 4.

Sample wt.% CFO	**Saturation magnetization (emu/g) at 20°C ± 0.1**	**Effective wt.% CFO at 20°C ± 0.1**
0.5	0.30	0.5
1	0.70	1.2
5	3.0	5.0
10	3.7	6.2
20	11.4	19.0
30	16.3	27.2

Table 1 shows that the effective wt.% of CFO is similar to the wt.% added to the polymer, except for the CFO/Carrageenan nanocomposite with 10 wt.% of NPs due to possible irregular distribution on the CFO nanoparticles for such concentration.

Figure 7c) shows the magnetic behavior of the CFO/carrageenan nanocomposite with 30 wt.% CFO content at three different temperatures (20, 50 and 100°C) where the magnetic hysteresis loops are found not to present a strong dependence of temperature variation. The magnetic saturation, remnant magnetization and coercive field slightly decrease with increasing temperature due to the thermally induced increase of the nanoparticles internal energy [52].

3.5. Magnetic actuator application

Considering the excellent magnetic properties of CFO/carrageenan nanocomposites, a multifunctional magnetic actuator has been manufactured and its response is represented in Figure 8. It is noticed that the coupling of the magnetic carrageenan-based actuator to piezoelectric films, allows to demonstrate sensing and energy harvesting capabilities. The device was produced with CFO/carrageenan nanocomposites with 30 wt.% of CFO, based on the larger magnetic response.

Figure 8 shows the amplified and filtered voltage response of the magnetic actuator when the NdFeB magnet approaches the multilayer system at 4 frequencies: 2.5, 1.5 1.2 and 0.8 Hz.

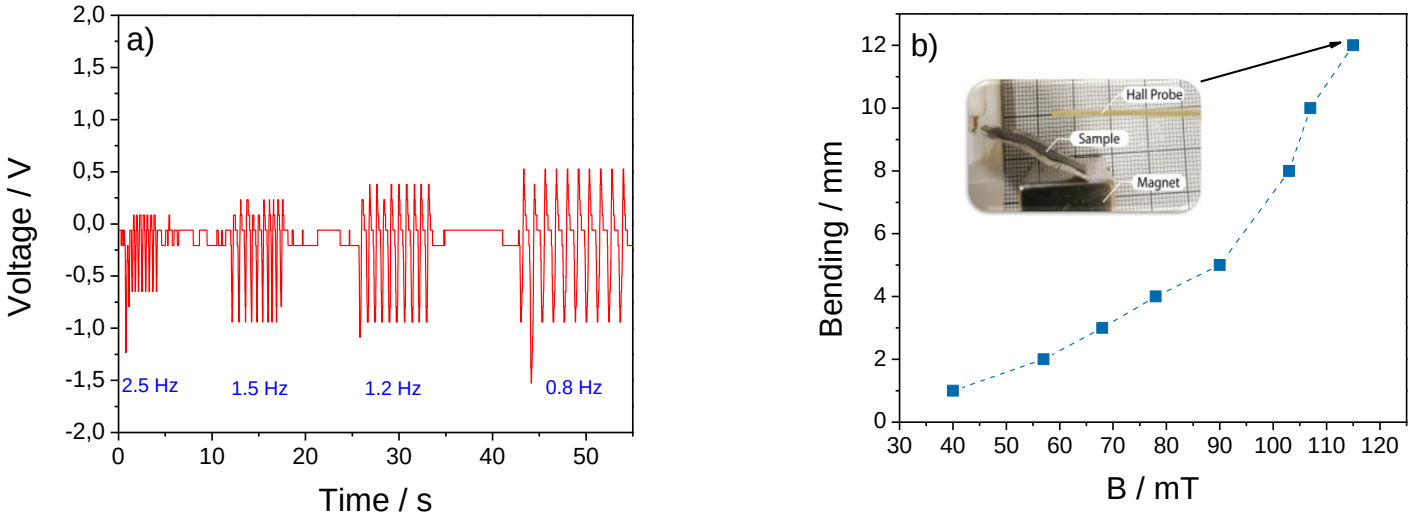

Figure 8 – a) Response of the magnetic actuator coupled to the piezoelectric film to the NdFeB magnet approach at 2,5 Hz, 1,5 Hz, 1,8 Hz, and 0,8 Hz. b) Actuation capability of the CFO/carrageenan-based device as a function of the magnetic field under static conditions.

The approximation of the magnet to the magnetoactive layer enables a bending movement of the multilayer system. The designed actuator, coupling the magnetic and piezoelectric

film, enables a voltage variation in the electrodes of the piezoelectric film, related to the magnetically activated bending of the magnetoactive carrageenan film. The electronic circuit translates that voltage variation as an increase in the maximum voltage of 0.5 V at 0.8 Hz (sensitivity of 8.3 $V.T^{-1}$). Figure 8a also shows that for lower frequencies the sensor achieves a higher amplitude that for higher frequencies, indicative of the low frequency response of the multilayer system (see video in Supporting Information).

Figure 8b represents the actuation capability of the device as a function of the induced magnetic field by moving the magnet closer to the sample from when the sample starts to react to the external magnetic field (at a field of 40 mT) and decreasing the distance to the sample until a maximum deformation was achieved. Due to the presence of the ferromagnetic CFO on the polymer matrix, the composite film is attracted to the magnetic field, being this attraction higher for higher magnetic fields. Based on the data presented in Fig. 8b, the bending of the samples corresponds to 104 $mm.T^{-1}$.

4. Conclusions

Magnetoactive cobalt ferrite $CoFe_2O_4$-CFO/Carrageenan nanocomposites were prepared using water as a solvent and processed by direct-ink-writing with different filler contents up to 30 wt.%.

A compact morphology is obtained for all films as well as a good dispersion of CFO nanoparticles in the carrageenan polymer matrix. The vibration bands of the carrageenan polymer were found to be independent of the CFO wt.%. Thermal and mechanical properties are both improved by the incorporation of the CFO nanoparticles in the carrageenan polymer matrix.

The dielectric and magnetic properties are also improved with the addition of CFO NPs, the dielectric constant increasing from ≈1000 for the pristine polymer to ≈9000 for the

10wt.% composite and a maximum magnetic response of ≈16 emu.g^{-1} saturation magnetization and ≈3.4 kOe coercive field were obtained for the polymer composites with 30wt.% filler content.

The functional response of the CFO/Carrageenan nanocomposites as magnetically active actuator were demonstrated in a multifunctional device capable of self-sensing actuation by binding to a piezoelectric polymer in a multilayer system, opening a new route to the development of environmentally friendlier IoT-related materials.

Acknowledgements

The authors thank the Fundação para a Ciência e Tecnologia (FCT) for financial support under the framework of Strategic Funding grants UIDB/04650/2020, UID/FIS/04650/2020 and UID/EEA/04436/2020, and under projects POCI-01-0145-FEDER-028157 and PTDC/FIS-MAC/ 28157/2017. The authors also thank the FCT for financial support under Grant SFRH/BD/131729/2017 (N.P.), and contracts CEECIND/03975/2017 (P.M) and 2020.04028.CEECIND (C.M.C.). Financial support from the Basque Government Industry Department under the ELKARTEK program is acknowledged. The authors thank for technical and human support provided by SGIker (UPV/EHU/ ERDF, EU).

References

[1] Y. Zhan, Y. Mei, L. Zheng, Materials capability and device performance in flexible electronics for the Internet of Things, Journal of Materials Chemistry C 2(7) (2014) 1220-1232.

[2] S. Phuyal, D. Bista, R. Bista, Challenges, Opportunities and Future Directions of Smart Manufacturing: A State of Art Review, Sustainable Futures 2 (2020) 100023.

[3] X.L. Zeng, Q.B. Song, J.H. Li, W.Y. Yuan, H.B. Duan, L.L. Liu, Solving e-waste problem using an integrated mobile recycling plant, Journal of Cleaner Production 90 (2015) 55-59.
[4] E. Kunnari, J. Valkama, M. Keskinen, P. Mansikkamäki, Environmental evaluation of new technology: printed electronics case study, Journal of Cleaner Production 17(9) (2009) 791-799.
[5] X. Wang, J. Zhang, X. Xia, C. Fang, G.J. Weng, Nonlinear magnetoelectric effects of polymer-based hybrid magnetoelectric composites with chain-like terfenol-D/epoxy and PVDF multilayers, Composites Science and Technology 216 (2021) 109069.
[6] J. Wiklund, A. Karakoç, T. Palko, H. Yiğitler, K. Ruttik, R. Jäntti, J. Paltakari, A Review on Printed Electronics: Fabrication Methods, Inks, Substrates, Applications and Environmental Impacts, Journal of Manufacturing and Materials Processing 5(3) (2021) 89.
[7] L.-Y. Zhou, J. Fu, Y. He, A Review of 3D Printing Technologies for Soft Polymer Materials, Advanced Functional Materials 30(28) (2020) 2000187.
[8] C. Bastioli, Biodegradable materials — Present situation and future perspectives, Macromolecular Symposia 135(1) (1998) 193-204.
[9] C. Aydemir, S. Özsoy, Environmental impact of printing inks and printing process, Journal of graphic engineering and design 11 (2020) 11-17.
[10] R. Barras, I. Cunha, D. Gaspar, E. Fortunato, R. Martins, L. Pereira, Printable cellulose-based electroconductive composites for sensing elements in paper electronics, Flexible and Printed Electronics 2(1) (2017) 014006.
[11] Y. Zhang, Y. Chen, Y. Jiang, G. Sui, Self-Thickening and Self-Strengthening 3D Printing Magnetic Cellulose-Based Aerogel for Adsorption and Recovery of Methylene Blue, Advanced Sustainable Systems 6 (3) (2022) 2100329.
[12] M. Atreya, K. Dikshit, G. Marinick, J. Nielson, C. Bruns, G.L. Whiting, Poly(lactic acid)-Based Ink for Biodegradable Printed Electronics With Conductivity Enhanced through Solvent Aging, ACS Applied Materials & Interfaces 12(20) (2020) 23494-23501.
[13] S.-N. Li, B. Li, Z.-R. Yu, L.-X. Gong, Q.-Q. Xia, Y. Feng, D. Jia, Y. Zhou, L.-C. Tang, Chitosan in-situ grafted magnetite nanoparticles toward mechanically robust and electrically conductive ionic-covalent nanocomposite hydrogels with sensitive strain-responsive resistance, Composites Science and Technology 195 (2020) 108173.

[14] N.A.A. Ghani, R. Othaman, A. Ahmad, F.H. Anuar, N.H. Hassan, Impact of purification on iota carrageenan as solid polymer electrolyte, Arabian Journal of Chemistry 12(3) (2019) 370-376.
[15] V. Moniha, M. Alagar, S. Selvasekarapandian, B. Sundaresan, G. Boopathi, Conductive bio-polymer electrolyte iota-carrageenan with ammonium nitrate for application in electrochemical devices, Journal of Non-Crystalline Solids 481 (2018) 424-434.
[16] A. George, P.A. Shah, P.S. Shrivastav, Natural biodegradable polymers based nano-formulations for drug delivery: A review, Int J Pharm 561 (2019) 244-264.
[17] T. Karbowiak, H. Hervet, L. Leger, D. Champion, F. Debeaufort, A. Voilley, Effect of plasticizers (water and glycerol) on the diffusion of a small molecule in iota-carrageenan biopolymer films for edible coating application, Biomacromolecules 7(6) (2006) 2011-9.
[18] E.-M. Pacheco-Quito, R. Ruiz-Caro, M.-D. Veiga, Carrageenan: Drug Delivery Systems and Other Biomedical Applications, Marine Drugs 18(11) (2020) 583.
[19] K.M. Zia, S. Tabasum, M. Nasif, N. Sultan, N. Aslam, A. Noreen, M. Zuber, A review on synthesis, properties and applications of natural polymer based carrageenan blends and composites, Int J Biol Macromol 96 (2017) 282-301.
[20] L. Li, R. Ni, Y. Shao, S. Mao, Carrageenan and its applications in drug delivery, Carbohydrate Polymers 103 (2014) 1-11.
[21] V. Moniha, M. Alagar, S. Selvasekarapandian, B. Sundaresan, R. Hemalatha, Development and Characterization of Bio-Polymer Electrolyte iota-carrageenan with Ammonium Salt for Electrochemical Application, Materials Today-Proceedings 8 (2019) 449-455.
[22] D. Bichiri, A.R. Rente, Â. Jesus, Safety and efficacy of iota-carrageenan nasal spray in treatment and prevention of the common cold, Medicine and pharmacy reports 94(1) (2021) 28-34.
[23] G. Song, Y. Shi, A. Li, H. Wang, G. Ding, Facile preparation of three-dimensional graphene oxide/ iota-carrageenan composite aerogel and its efficient ability for selective adsorption of methylene blue, Journal of Materials Science 56(26) (2021) 14866-14879.
[24] L. Pereira, Extracção, caracterização e utilização das carragenanas, PhD thesis (2010).
[25] V. Moniha, M. Alagar, S. Selvasekarapandian, B. Sundaresan, R. Hemalatha, G. Boopathi, Synthesis and characterization of bio-polymer electrolyte based on iota-

carrageenan with ammonium thiocyanate and its applications, Journal of Solid State Electrochemistry 22(10) (2018) 3209-3223.
[26] T. Sugumaran, D.S. Silvaraj, N.M. Saidi, N.K. Farhana, S. Ramesh, K. Ramesh, S. Ramesh, The conductivity and dielectric studies of polymer electrolytes based on iota-carrageenan with sodium iodide and 1-butyl-3-methylimidazolium iodide for the dye-sensitized solar cells, Ionics 25(2) (2019) 763-771.
[27] M. Bener, F.B. Sen, A. Kasgoz, R. Apak, Carrageenan-based colorimetric sensor for total antioxidant capacity measurement, Sensor Actuat B-Chem 273 (2018) 439-447.
[28] C.-F. Hung, C.-C. Chen, P.-C. Yeh, P.-W. Chen, T.-K. Chung, A magnetic-piezoelectric smart material-structure sensing three axis DC and AC magnetic-fields, Applied Physics A 123(12) (2017) 739.
[29] K.J. Merazzo, A.C. Lima, M. Rincón-Iglesias, L.C. Fernandes, N. Pereira, S. Lanceros-Mendez, P. Martins, Magnetic materials: a journey from finding north to an exciting printed future, Materials Horizons 8(10) (2021) 2654-2684.
[30] S. Munjal, N. Khare, Transforming single domain magnetic CoFe2O4 nanoparticles from hydrophobic to hydrophilic by novel mechanochemical ligand exchange, Journal of Nanoparticle Research 19(1) (2017) 18.
[31] F. Sharifianjazi, M. Moradi, N. Parvin, A. Nemati, A.J. Rad, N. Sheysi, A. Abouchenari, A. Mohammadi, S. Karbasi, Z. Ahmadi, A. Esmaeilkhanian, M. Irani, A. Pakseresht, S. Sahmani, M.S. Asl, Magnetic CoFe2O4 nanoparticles doped with metal ions: A review, Ceramics International 46(11) (2020) 18391-18412.
[32] C. Cheng, J. Dai, Z. Li, W. Feng, Preparation and Magnetic Properties of CoFe2O4 Oriented Fiber Arrays by Electrospinning, Materials (Basel) 13(17) (2020) 3860.
[33] S. Munjal, N. Khare, C. Nehate, V. Koul, Water dispersible CoFe2O4 nanoparticles with improved colloidal stability for biomedical applications, Journal of Magnetism and Magnetic Materials 404 (2016) 166-169.
[34] H. Verma, T. Mekuria, P. Seck, H. Hong, S.P. Karna, D. Seifu, Proximity effect tuned magnetic properties in composites of carbon nanotubes and nanoparticles of CoFe2O4, Journal of Magnetism and Magnetic Materials 501 (2020) 166438.
[35] T. Mekuria, S. Khalid, K. Krycka, M. Bleuel, H. Verma, H. Hong, S.P. Karna, D. Seifu, Cobalt ferrite nanoparticle intercalated carbon nanotubes for a nanomagnetic ultrasensitive sensor of Cr-VI in water, AIP Advances 10(6) (2020) 065134.

[36] C.G. Kaufmann Junior, R.Y.S. Zampiva, A.K. Alves, C.P. Bergmann, L. Giorgini, Synthesis of cobalt ferrite (CoFe2O4) by combustion with different concentrations of glycine, IOP Conference Series: Materials Science and Engineering 659 (2019) 012079.
[37] X. Mu, H. Zhang, C. Zhang, S. Yang, J. Xu, Y. Huang, J. Xu, Y. Zhang, Q. Li, X. Wang, D. Cao, S. Li, Poly(vinylidene fluoride-trifluoroethylene)/cobalt ferrite composite films with a self-biased magnetoelectric effect for flexible AC magnetic sensors, Journal of Materials Science 56(16) (2021) 9728-9740.
[38] M. Lanús Mendez Elizalde, C. Acha, F.V. Molina, P.S. Antonel, Composites of Poly(3,4-ethylenedioxythiophene) and CoFe2O4 Nanoparticles: Composition Influence on Structural, Electrical, and Magnetic Properties, The Journal of Physical Chemistry C 124(12) (2020) 6884-6895.
[39] F. Kremer, A. Schönhals, Broadband Dielectric Spectroscopy, Springer2003.
[40] S. Gonçalves, J. Serrado-Nunes, J. Oliveira, N. Pereira, L. Hilliou, C.M. Costa, S. Lanceros-Méndez, Environmentally Friendly Printable Piezoelectric Inks and Their Application in the Development of All-Printed Touch Screens, ACS Applied Electronic Materials 1(8) (2019) 1678-1687.
[41] L. Pereira, A.M. Amado, A.T. Critchley, F. Van de Velde, P.J. Ribeiro-Claro, Identification of selected seaweed polysaccharides (phycocolloids) by vibrational spectroscopy (FTIR-ATR and FT-Raman), Food Hydrocolloids 23(7) (2009) 1903-1909.
[42] N.G. Rajasulochana, Analysis on the Seasonal Variations in Carrageenans of Hypnea flagelliformis and Sarconema filiforme by FTIR Spectroscopy. , Asian Journal of Chemistry. 21 (2009) 4547-4552.
[43] M. Kamranifar, A. Allahresani, A. Naghizadeh, Synthesis and characterizations of a novel CoFe2O4@CuS magnetic nanocomposite and investigation of its efficiency for photocatalytic degradation of penicillin G antibiotic in simulated wastewater, J Hazard Mater 366 (2019) 545-555.
[44] R. Fu, Y. Yan, C. Roberts, Z. Liu, Y. Chen, The role of dipole interactions in hyperthermia heating colloidal clusters of densely-packed superparamagnetic nanoparticles, Scientific Reports 8(1) (2018) 4704.
[45] F.N. Jumaah, N.N. Mobarak, A. Ahmad, M.A. Ghani, M.Y.A. Rahman, Derivative of iota-carrageenan as solid polymer electrolyte, Ionics 21(5) (2014) 1311-1320.
[46] K. Mitsuda, H. Kimura, T. Murahashi, Evaporation and Decomposition of Triton-X-100 under Various Gases and Temperatures, Journal of Materials Science 24(2) (1989) 413-419.

[47] C.M. Costa, V. Sencadas, I. Pelicano, F. Martins, J.G. Rocha, S. Lanceros-Méndez, Microscopic origin of the high-strain mechanical response of poled and non-poled poly (vinylidene fluoride) in the β-phase, Journal of non-crystalline solids 354(32) (2008) 3871-3876.
[48] J.Y. Kim, S.I. Han, D.K. Kim, S.H. Kim, Mechanical reinforcement and crystallization behavior of poly(ethylene 2,6-naphthalate) nanocomposites induced by modified carbon nanotube, Composites Part A: Applied Science and Manufacturing 40(1) (2009) 45-53.
[49] M. Samet, V. Levchenko, G. Boiteux, G. Seytre, A. Kallel, A. Serghei, Electrode polarization vs. Maxwell-Wagner-Sillars interfacial polarization in dielectric spectra of materials: Characteristic frequencies and scaling laws, The Journal of Chemical Physics 142(19) (2015) 194703.
[50] P. Kumar, S.K. Sharma, M. Knobel, M. Singh, Effect of La3+ doping on the electric, dielectric and magnetic properties of cobalt ferrite processed by co-precipitation technique, Journal of Alloys and Compounds 508(1) (2010) 115-118.
[51] R. Taherian, A. Kausar, Electrical Conductivity in Polymer-Based Composites: Experiments, Modelling, and Applications, William Andrew2018.
[52] A. Reizabal, C.M. Costa, N. Pereira, L. Pérez-Álvarez, J.-L. Vilas-Vilela, S. Lanceros-Méndez, Silk Fibroin Based Magnetic Nanocomposites for Actuator Applications, Advanced Engineering Materials 22(6) (2020) 2000111.
[53] P. Martins, J.S. Nunes, J. Oliveira, N. Peřinka, S. Lanceros-Mendez, Spray-printed magnetoelectric multifunctional composites, Composites Part B: Engineering 187 (2020) 107829.
[54] M. Rajendran, R.C. Pullar, A.K. Bhattacharya, D. Das, S.N. Chintalapudi, C.K. Majumdar, Magnetic properties of nanocrystalline CoFe2O4 powders prepared at room temperature: variation with crystallite size, Journal of Magnetism and Magnetic Materials 232(1) (2001) 71-83.
[55] M. Guillot-Ferriols, J.C. Rodriguez-Hernandez, D.M. Correia, S.A.C. Carabineiro, S. Lanceros-Mendez, J.L. Gomez Ribelles, G. Gallego Ferrer, Poly(vinylidene) fluoride membranes coated by heparin/collagen layer-by-layer, smart biomimetic approaches for mesenchymal stem cell culture, Mater Sci Eng C Mater Biol Appl 117 (2020) 111281.